

Measurements of Electron Temperature and Density Distribution on a V-Shaped Target of a Divertor Simulation Experimental Module in GAMMA 10/PDX

Kensuke OKI, Mizuki SAKAMOTO, Yousuke NAKASHIMA, Motoki YOSHIKAWA, Kunpei NOJIRI, Ryo NOHARA, Akihiro TERAKADO, Masayuki YOSHIKAWA, Junko KOHAGURA, Hisato TAKEDA, Kazuya ICHIMURA, Tsuyoshi IMAI and Makoto ICHIMURA

Plasma Research Center, University of Tsukuba, Tsukuba, Ibaraki 305-8577, Japan

(Received 16 July 2014 / Accepted 18 May 2015)

Spatial distributions of electron temperature and density have been measured using Langmuir probes on a tungsten V-shaped target plate of a divertor simulation experimental module in GAMMA 10/PDX. In standard hot-ion plasmas, the electron temperature is about 30–50 eV, which is comparable to that in confined core plasmas. The electron density is on the order of 10^{16} m^{-3} but increases about 3 times owing to additional ion cyclotron range of frequency heating. In a direction along the target plate toward the corner, the electron temperature seems to slightly decrease toward the corner. In another direction perpendicular to this direction, the electron temperature profile seems to be roughly flat. The profile of electron density compensated for the expansion of magnetic flux tubes is similar to the core plasma, but the compensated density decreases near the corner. As the open angle of the target decreases, the compensated density decreases although the electron temperature does not change much. These density decreases may be due to increase in flow velocity caused by electric and pressure forces in the pre-sheath.

© 2015 The Japan Society of Plasma Science and Nuclear Fusion Research

Keywords: divertor simulation experiment, GAMMA 10/PDX, Langmuir probe, electron temperature, electron density, V-shaped tungsten target plate, spatial distribution at a target plate, plasma–wall interaction

DOI: 10.1585/pfr.10.1402071

1. Introduction

It is important to understand divertor physics and plasma–wall interaction (PWI) such as impurity transport and radiation cooling for the detachment to reduce the heat load on a divertor plate [1]. In the large tandem mirror device GAMMA 10/PDX, divertor simulation experiments have been conducted using an end region with an open magnetic field configuration [2–4]. One of the advantages of GAMMA 10/PDX over other small divertor simulators is existence of confined core plasma with high ion and electron temperatures up to $\sim 10 \text{ keV}$ and $\sim 100 \text{ eV}$, respectively [5]. Another advantage is its large pumping capability. Moreover, GAMMA 10/PDX has various high-power heating systems, i.e., electron cyclotron heating (ECH), ion cyclotron range of frequency (ICRF), and neutral beam injection (NBI), which lead to good controllability of plasma parameters and the ITER-relevant heat flux to the end region. Recently, a divertor simulation experimental module (D-module) has been installed at the end region [6, 7]. A variety of experiments for divertor physics and PWI can be performed using the D-module.

In this study, electron temperature T_e and density n_e of plasmas in the D-module have been measured using Lang-

muir probes on a target plate in order to characterize the divertor simulation plasmas. In particular, spatial distributions of the electron temperature and density at the target plate are reported.

2. Experimental Apparatus

Figure 1 shows schematic views of GAMMA 10/PDX and the D-module. The D-module consists of a stainless-steel rectangular parallelepiped chamber (cross-section of $480 \text{ mm} \times 500 \text{ mm}$, 700 mm in length) with an inlet with diameter of 200 mm (which is narrowed by a tungsten limiter as shown in Fig. 1 (c)) and two tungsten plates ($350 \text{ mm} \times 300 \text{ mm} \times 0.2 \text{ mm}$) forming a V-shape with their open angle of $15\text{--}80$ degrees. A gas injection system is installed in the D-module for radiation cooling and detachment studies. At the back of the D-module, an exhaust door for pumping is attached with adjustable conductance. In this study, we did not use the gas injection system and the exhaust door was closed. The chamber of the D-module and the target plate were electrically connected with each other and floating from the earth. The vacuum vessel of GAMMA 10/PDX is electrically connected to the earth.

Thirteen Langmuir probes (single probes) are installed on the upper plate of the V-shaped target as shown in Fig. 2.

author's e-mail: oki@prc.tsukuba.ac.jp

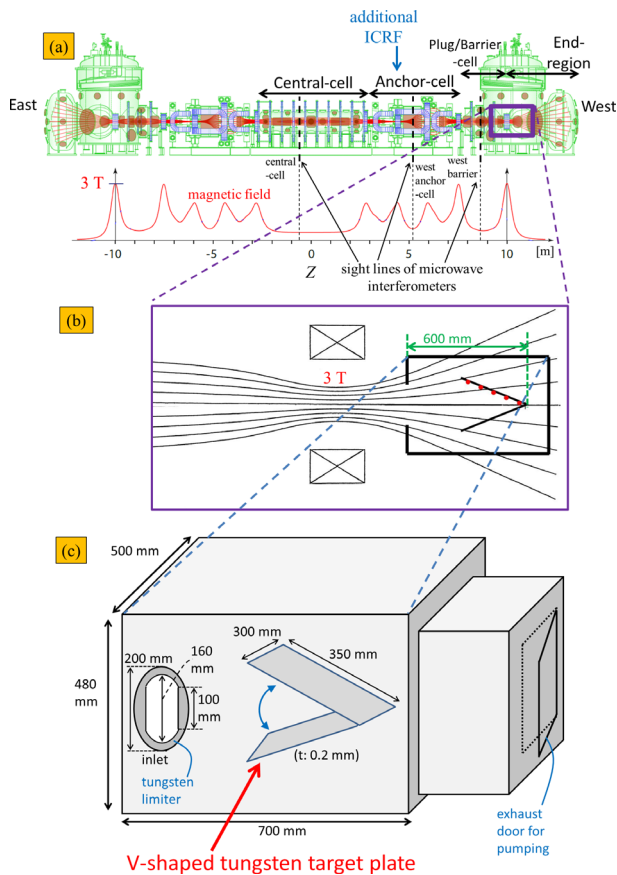


Fig. 1 Schematic views of (a) GAMMA 10/PDX and its axial (Z) magnetic field profile, (b) the D-module and magnetic field line configuration, and (c) details of the D-module.

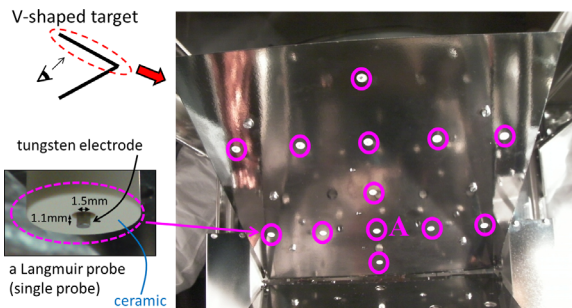


Fig. 2 Photographs of the Langmuir probes on the V-shaped target plate.

The probe electrode is made of tungsten with diameter of 1.5 mm and length of 1.1 mm. Sine-wave sweep voltages from -200 to 140 V at 50 Hz are applied to the Langmuir probes separately, where potential of 0 V is the potential of the target plate. The electron density is evaluated using the electron saturation current. Here, the electron collection area of the probe is assumed to be the projection area (one-side) to the magnetic field direction.

3. Experimental Results

Figure 3 shows typical time evolution of parameters of a mirror-confined core plasma in the central-cell, west anchor-cell, and west barrier region and the electron temperature T_e and density n_e measured using the Langmuir probe denoted as A in Fig. 2. The error bars of T_e and n_e at the target plate are evaluated from uncertainty of curve fitting of voltage–current characteristics, circuit elements (isolation amplifiers, analog to digital converters, resistive voltage dividers, and shunt resistors), and the probe area. In this discharge, standard hot-ion plasma (ion temperature is $\sim 1\text{--}10$ keV in the central-cell) was generated and sustained by ICRF in the central-cell and the west and east anchor-cells. ECH and NBI were not applied. Additional ICRF in the west anchor region was applied from 160 ms to 240 ms. Owing to the additional ICRF, the electron temperature slightly decreased and density increased both in the core plasma and at the target plate. It is found that the electron temperature at the target plate is comparable to that in the core plasma. On the other hand, the electron density at the target plate is rather lower than that in the central-cell.

Figure 4 shows spatial distributions of the electron temperature and density in the L direction, which is along the upper plate toward the corner of the V-shape, at the period with the additional ICRF for the open angles of 60 , 45 , and 30 degrees. For each of the open angles, the electron temperature seems to slightly decrease toward the corner. As the open angle decreases, the electron density decreases near the corner ($L = -35$ mm and -105 mm) and increases near the tip of the target plate ($L = -245$ mm and -315 mm).

Figure 5 shows spatial distributions of the electron temperature and density in the Y direction, which is perpendicular to the L direction, at the period with the additional ICRF. The distribution of the electron temperature seems to be roughly flat, although the electron temperature at $Y = +120$ mm seems to be slightly high. The electron density seems to have a peak near $Y = -60$ mm. As the open angle decreases, the electron density decreases at $Y = -60$ mm and 0 mm.

4. Discussion

In Fig. 3, the line-averaged electron density in the west barrier region is one to two orders of magnitude lower than the central and anchor cells. The electron density at the target plate is of the same order of magnitude as the line-averaged density in the west barrier region. Thus, the large density drop from the central-cell to the target is considered to be due to the mirror confinement between the west anchor-cell and the west plug/barrier-cell.

With the additional ICRF, although the electron densities in the central and west anchor cells increased about 1.2 to 1.4 times, the electron densities in the west barrier region and at the target increased as much as about 3 times.

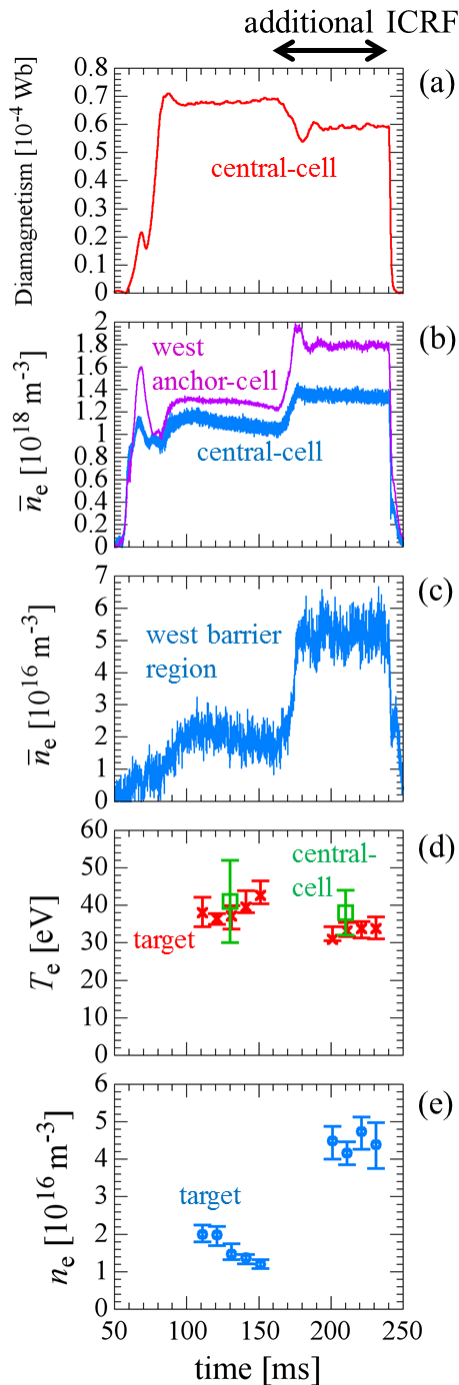


Fig. 3 Typical time evolution of (a) diamagnetism in the central-cell, (b) line-averaged electron density \bar{n}_e in the central-cell (blue line) and in the west anchor-cell (purple line), (c) line-averaged electron density \bar{n}_e in the west barrier region, (d) electron temperature T_e measured using Thomson scattering on the axis in the central-cell (green squares denote results of two similar shots) and measured using the Langmuir probe on the target plate (red crosses), and (e) electron density n_e measured using the Langmuir probe on the target plate. These line-averaged electron densities are evaluated from line-integrated electron densities measured using the microwave interferometers (Fig. 1 (a)) and plasma diameters determined by the central-cell limiter with diameter of 0.36 m. The open angle of the target plate was 45 degrees.

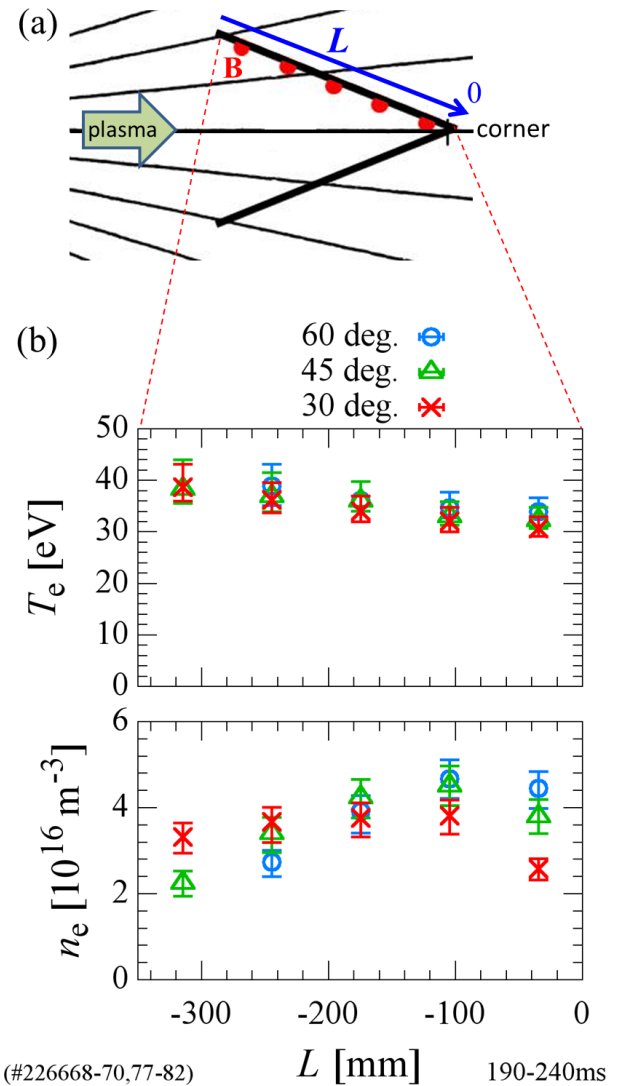


Fig. 4 (a) Illustration of the L direction with a side view of the V-shaped target plate, probe positions (red dots), and magnetic field lines. (b) Distributions of electron temperature T_e and density n_e in the L direction (at the center line of the plate) with the additional ICRF (each point is the average over 190 to 240 ms of three shots).

The axial loss rate from the mirror confinement region of the west anchor-cell to that of the west plug/barrier-cell is considered to change owing to the additional ICRF. Further additional wave heating systems are expected to be useful for higher density near the target plate.

For further comparison of the distributions for different open angles shown in Figs. 4 and 5, we convert the horizontal axis of these graphs to a radial coordinate. We express this radial coordinate by using R_{CC} which is the projected radial position from the probe to the central-cell along the magnetic field line. In Figs. 6 and 7, the plotted data are the same as in Figs. 4 and 5, respectively, but the horizontal axis is converted to R_{CC} . Moreover, in Figs. 6 and 7, the electron density is converted in order to compensate for the density decrease due to the radial expansion

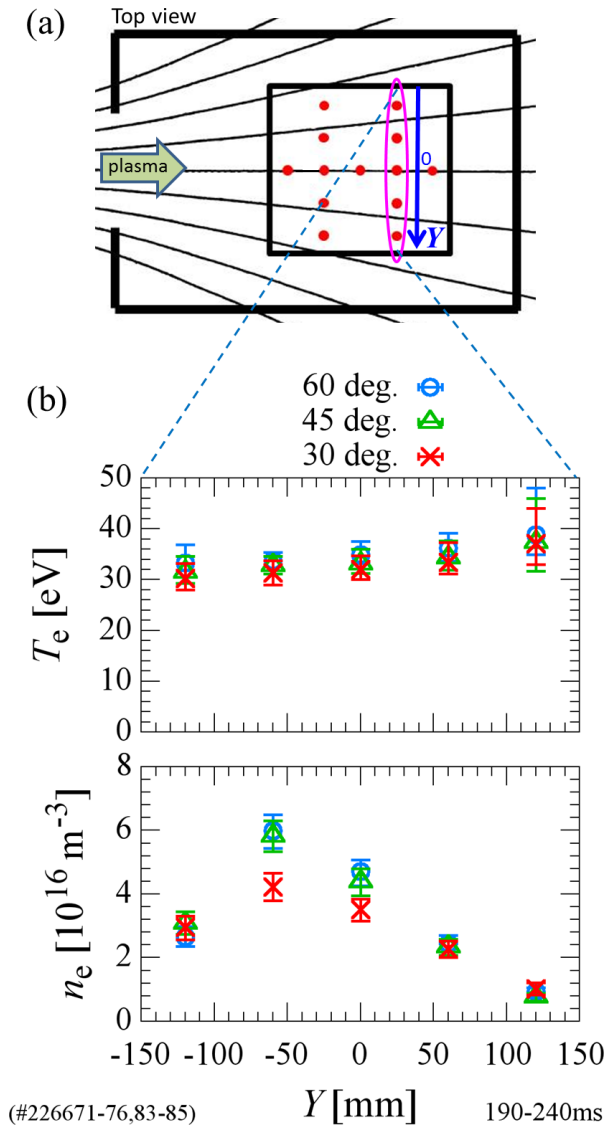


Fig. 5 (a) Illustration of the Y direction with a top view of the V-shaped target plate, probe positions (red dots), D-module, and magnetic field lines (projection on the mid-plane). (b) Distributions of electron temperature T_e and density n_e in the Y direction on the target plate with the additional ICRF (each point is the average over 190 to 240 ms of three shots).

of the magnetic field lines. For this compensated density $n_{e(c)}$, we considered the followings. The particle conservation equation in the flux tube shown in Fig. 8 is

$$\int_{\text{flux-tube}} \frac{dn_e}{dt}(\text{source})dV = n_{e(\text{probe})}u_{\text{probe}}S_{\text{probe}} - n_{e(\text{ref})}u_{\text{ref}}S_{\text{ref}}, \quad (1)$$

where the left-hand side is the integral of the electron source term in the flux tube volume V , u is flow velocity, S is the cross-sectional area of the flux tube, and subscripts “probe” and “ref” denote the probe position and a reference axial position, respectively. We set the reference axial position to the axial position of the most upstream

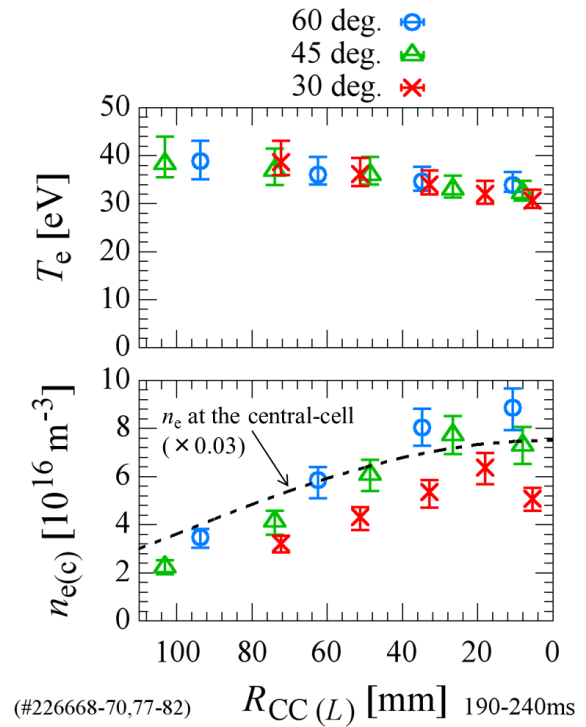


Fig. 6 Distributions of electron temperature T_e and converted electron density $n_{e(c)}$ to compensate for the expansion of the magnetic flux tubes with R_{CC} of the probe position in the L direction array which corresponds to Fig. 4. The dashed line is the n_e profile at the central-cell (multiplied by 0.03).

probe (B in Fig. 4 (a)) in the case of the open angle of 45 degrees. Regarding the electron source term, ionization dominates over recombination because T_e is 30–50 eV. We estimate that the order of the left-hand side of Eq. (1) is $\int_{\text{flux-tube}} n_e n_H \langle \sigma v \rangle dV \sim n_e n_H (3 \times 10^{-14} \text{ m}^3 \text{ s}^{-1}) S (0.1 \text{ m})$, where n_H is the density of the neutral hydrogen (atoms and molecules), $\langle \sigma v \rangle \sim 3 \times 10^{-14} \text{ m}^3 \text{ s}^{-1}$ is the rate coefficient of the electron impact ionization (p. 35 of [8]), and the length of the flux tube is $\sim 0.1 \text{ m}$. The order of the right-hand side of Eq. (1) is $\sim n_e (2 \times 10^5 \text{ ms}^{-1}) S$, where the order of u is estimated from the ion sound speed of $\sim 2 \times 10^5 \text{ ms}^{-1}$ for $T_e = 40 \text{ eV}$ and a typical ion temperature of 400 eV. Therefore, if n_H is lower than about 10^{18} m^{-3} , the left-hand side of Eq. (1) can be ignored compared with the right-hand side of Eq. (1). When recycled neutral particles from the target are not taken into account, n_H is lower than 10^{18} m^{-3} for the standard gas-puff condition in this study. We roughly estimate the density of the recycled neutral particles from the target taking the following steps. The ion flux to the target is about $2 \times 10^{16} \text{ m}^{-3} \times 2 \times 10^5 \text{ ms}^{-1} = 4 \times 10^{21} \text{ m}^{-2} \text{ s}^{-1}$, which corresponds to the measured ion saturation current. We assume that the particle recycling coefficient of the target is 1 and that the plasma-wetted target area projected to the magnetic field direction is about $0.35 \text{ m} \times 0.3 \text{ m} \times 2 \times \sin(28 \text{ deg.}) = 0.0986 \text{ m}^2$ (28 deg.

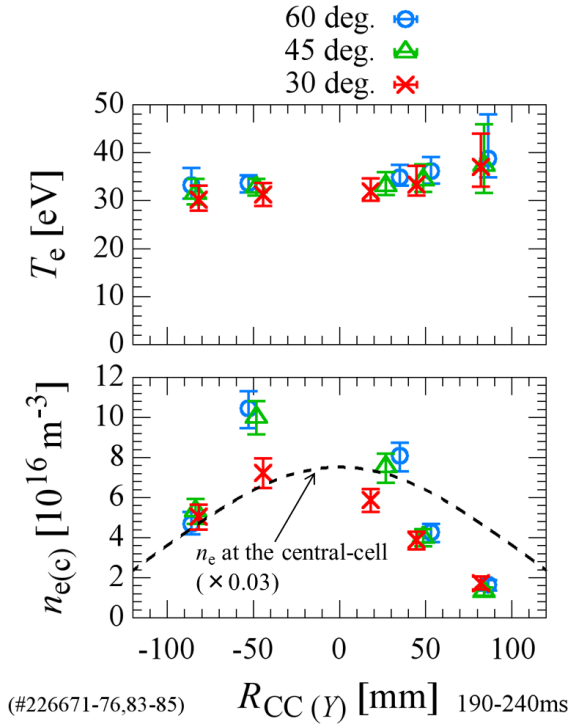


Fig. 7 Distributions of electron temperature T_e and converted electron density $n_{e(c)}$ to compensate for the expansion of the magnetic flux tubes with R_{CC} of the probe position in the Y direction array which corresponds to Fig. 5. In the horizontal axis, $R_{CC} < 0$ corresponds to $Y < 0$ and $R_{CC} > 0$ corresponds to $Y \geq 0$. The dashed line is the n_e profile at the central-cell (multiplied by 0.03).

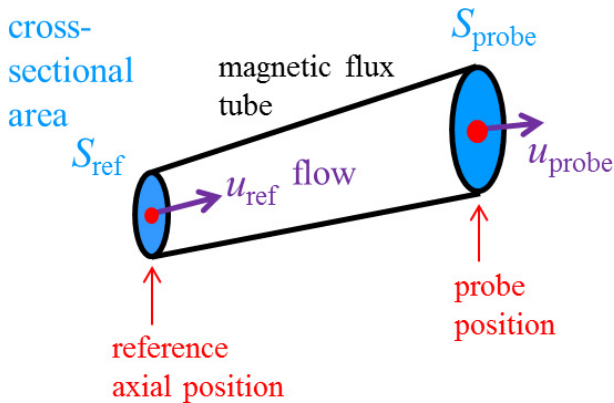


Fig. 8 Schematic of a magnetic flux tube between a reference axial position and a probe position.

is roughly the angle between the magnetic field line and the target plate when the open-angle is 45 deg.). Then, the number of the recycled neutral particles released from the target per unit time is $4 \times 10^{21} \text{ m}^{-2} \text{ s}^{-1} \times 0.0986 \text{ m}^2 = 3.9 \times 10^{20} \text{ s}^{-1}$. Because the total volume of the vacuum vessel of the plug/barrier and end region outside the D-module is $> 30 \text{ m}^3$ and much larger than that of the D-module (0.17 m^3), recycled neutral particle density outside

the D-module is much lower than that inside the D-module. Thus, the net number of recycled neutral particles escaping from the D-module through the inlet per unit time is considered to be $n_H A v_n / 4$, where n_H is recycled neutral particle density inside the D-module, A is the area of the inlet, and v_n is average velocity of the recycled neutral particles. In the quasi-steady state, this number of escaping neutral particles is balanced with the number of the recycled neutral particles released from the target per unit time, i.e.,

$$n_H A v_n / 4 = 3.9 \times 10^{20} [\text{s}^{-1}]. \quad (2)$$

A certain fraction of the recycled neutral particles were directly back-scattered or reflected from the target with some fraction of the impact energy of the incident ions and have velocity near the ion sound speed $v_i \sim 2 \times 10^5 \text{ m/s}$. The energy reflection coefficient is about 0.3 for a tungsten target and incident hydrogen ion with energy of 400 eV according to Fig. 3.2 in the page 113 of [8] (the mass ratio is 184 and the reduced energy ε is 0.0405). Thus, several tens percent of the neutral particles released from the target may have velocity near the ion incident velocity. The other fraction of neutral particles released from the target are considered to have average velocity for temperature of the target plate, which is $v_t \sim 2.4 \times 10^3 \text{ m/s}$ (the temperature of the target plate is about 280 K in this experiment). Some of the neutral particles released from the target with the velocity near v_t are accelerated to the ion velocity by the charge exchange. The mean free path for this charge exchange process is $v_i / (\langle \sigma v_{i-n} \rangle n_i)$, where $v_{i-n} \sim v_i$ is relative velocity between the neutral particles and ions (which corresponds to 400 eV), $\langle \sigma v_{i-n} \rangle \sim 8 \times 10^{-14} \text{ m}^3 \text{ s}^{-1}$ is the rate coefficient of the charge exchange (p. 35 of [8]), and $n_i \sim n_e \sim 4 \times 10^{16} \text{ m}^{-3}$ is the ion density. This mean free path is about 0.75 m, which is comparable to the length of the D-module (0.7 m). Thus, there is the possibility that several tens percent of the released neutral particles are accelerated to the ion velocity (near v_i) by the charge exchange in the D-module. We let the fraction of the recycled neutral particles having the velocity near v_i (owing to the reflection from the target or the charge exchange) be k_i (0–1). The left-hand side of Eq. (2) can be expressed as $n_H A (k_i v_i + (1 - k_i) v_t) / 4$; thus,

$$n_H = 3.9 \times 10^{20} [\text{s}^{-1}] \times 4 / (A (k_i v_i + (1 - k_i) v_t)). \quad (3)$$

Here A is 0.017 m^2 . As k_i increases, n_H decreases. For $k_i = 0$, n_H becomes maximum of $\sim 3.8 \times 10^{19} \text{ m}^{-3}$. However, for $k_i > 0.22$, n_H is $< 2 \times 10^{18} \text{ m}^{-3}$. For $k_i > 0.45$, n_H is $< 1 \times 10^{18} \text{ m}^{-3}$. Therefore, there is the possibility that n_H is lower than about $1\text{--}2 \times 10^{18} \text{ m}^{-3}$. Note that the plasma screening is not considered in this rough estimation. On the other hand, in another gas injection experiment where the H_2 gas density was $\sim 5 \times 10^{19} \text{ m}^{-3}$, the $\text{H}\alpha$ line intensity increased about 30 times, n_e increased about 3 times, and T_e did not change much (the excitation rate coefficient for $\text{H}\alpha$ remained almost unchanged) in the D-module. Thus,

in the no gas injection experiments of this paper, n_H may be about $5 \times 10^{18} \text{ m}^{-3}$. If n_H is $5 \times 10^{18} \text{ m}^{-3}$, the left-hand side of Eq. (1) is one or two orders of magnitude lower than the right-hand side. Thus, Eq. (1) may become

$$n_{e(\text{ref})} u_{\text{ref}} S_{\text{ref}} = n_{e(\text{probe})} u_{\text{probe}} S_{\text{probe}}. \quad (4)$$

According to Eq. (4), if u is spatially uniform ($u_{\text{ref}} = u_{\text{probe}}$), $n_{e(\text{probe})} S_{\text{probe}} / S_{\text{ref}}$ is electron density at the reference axial position. We use this value as the compensated density, i.e., $n_{e(c)} = n_{e(\text{probe})} S_{\text{probe}} / S_{\text{ref}}$. We can express the radial density distribution at the reference axial position by the radial $n_{e(c)}$ distribution under the assumption that u is spatially uniform ($u_{\text{ref}} = u_{\text{probe}}$) and the assumption that there is almost neither source nor sink of electrons in the flux tube (or the order of n_H is lower than about 10^{18} m^{-3}).

In Figs. 6 and 7, n_e profile at the central-cell is also shown. The $n_{e(c)}$ profile at the target plate is similar to this n_e profile at the central-cell where n_e increases toward the axis. However, $n_{e(c)}$ decreases near the corner especially for the small open angle. Moreover, $n_{e(c)}$ decreases as the open angle decreases. These decreases in $n_{e(c)}$ are considered to be due to increase in u toward the target. That is, the above-mentioned assumption of spatially uniform u is considered not to be valid near the target. Decrease in electron density toward the target was observed also in APSEDAS [9] and PSI-2 [10]. The reason for the density decrease near the target is considered to be ion acceleration due to electric and pressure forces in the pre-sheath region [10]. The same mechanism is expected to exist in the D-module. This pre-sheath effect may be higher near the corner and for the small open angles.

Another cause of the change in u is the expansion of the magnetic field lines. Single-particle velocity parallel to the magnetic field v_{\parallel} increases owing to the decrease in the magnetic field strength B without any collision and electric force. By conservation of kinetic energy and magnetic moment, this increase in v_{\parallel} from the reference axial position to the probe position is

$$\begin{aligned} \frac{v_{\parallel(\text{probe})}}{v_{\parallel(\text{ref})}} &= \sqrt{\frac{1 + \frac{v_{\parallel(m)}^2}{v_{\perp(m)}^2} - \frac{B_{(\text{probe})}}{B_{(m)}}}{1 + \frac{v_{\parallel(m)}^2}{v_{\perp(m)}^2} - \frac{B_{(\text{ref})}}{B_{(m)}}}} \\ &\leq \sqrt{\frac{1 - \frac{B_{(\text{probe})}}{B_{(m)}}}{1 - \frac{B_{(\text{ref})}}{B_{(m)}}}}, \end{aligned} \quad (5)$$

where v_{\perp} is velocity perpendicular to the magnetic field, $B_{(\text{probe})}$ is lower than $B_{(\text{ref})}$, and subscript (m) denotes the position of the maximum magnetic field strength, i.e., the mirror throat ($B_{(m)} = 3 \text{ T}$, see Fig. 1 (b)). Here, $B_{(\text{ref})}$ is about 0.3 T and $B_{(\text{probe})}$ is higher than about 0.15 T. The maximum value of Eq. (5) is only about 1.03, which is low when compared with the error bars of $n_{e(c)}$. Therefore, we

can ignore its effect on the interpretation of the measured $n_{e(c)}$.

The distribution of the electron temperature does not change much when the open angle changes as shown in Figs. 6 and 7. On the other hand, the electron temperature seems to slightly decrease toward the axis (corner). This is opposite to the usual radial profile in the core plasma where the temperature increases toward the axis. Therefore, this distribution in the L direction suggests that the electron temperature may decrease along the magnetic field direction. A reason for this decrease in the electron temperature may be collisions with the recycled neutral particles from the target. These collisions are associated with excitation and ionization. One may argue that ionization increases the electron density near the corner, which does not correspond to the measured $n_{e(c)}$ profile. However, the density decrease due to the increase in the flow velocity may dominate over the density increase due to ionization, as previously discussed about Eq. (1). Another reason for the decrease in the electron temperature may be decrease in the ion temperature due to the charge exchange with the recycled neutral particles and reduction in the energy transfer from ions to electrons.

5. Conclusion

In order to characterize the plasmas, the spatial distributions of the electron temperature and density have been measured using the Langmuir probes on the V-shaped target plate of the D-module in GAMMA 10/PDX. In standard hot-ion plasmas, the electron temperature is from $\sim 30 \text{ eV}$ to $\sim 50 \text{ eV}$, which is comparable to the core plasma. The electron density is on the order of 10^{16} m^{-3} . This lower density than the central-cell seems to be caused by the mirror confinement. The additional ICRF has increased the electron density at the target plate as much as about 3 times. Further additional wave heating systems are expected to be useful for higher density.

In the L direction distribution, the electron temperature seems to slightly decrease toward the corner. The distribution of the electron temperature in the Y direction seems to be roughly flat. The electron temperature does not depend on the open angle of the V-shaped target much. The profile of the electron density compensated for the expansion of the magnetic flux tubes is similar to the core plasma where the density increases toward the axis. However, the compensated density decreases near the corner and at the small open angle, suggesting density decrease toward the target plate. This may be due to the increase in the flow velocity caused by electric and pressure forces in the pre-sheath.

Acknowledgments

This work was partially supported by the NIFS Collaborative programs (NIFS12KUGM066, NIFS13KUGM083, and NIFS14KUGM086).

- [1] G.F. Matthews, *J. Nucl. Mater.* **220–222**, 104 (1995).
- [2] Y. Nakashima *et al.*, *Fusion Eng. Des.* **85**, 956 (2010).
- [3] Y. Nakashima *et al.*, *J. Nucl. Mater.* **415**, S996 (2011).
- [4] Y. Nakashima *et al.*, *J. Nucl. Mater.* **438**, S738 (2013).
- [5] T. Tamano, *Phys. Plasmas* **2**, 2321 (1995).
- [6] Y. Nakashima *et al.*, *Trans. Fusion Sci. Technol.* **63**, 1T, 100 (2013).
- [7] M. Sakamoto *et al.*, *Trans. Fusion Sci. Technol.* **63**, 1T, 188 (2013).
- [8] P.C. Stangeby, *The Plasma Boundary of Magnetic Fusion Devices* (Taylor & Francis Group, New York, 2000) p.35, 111–114.
- [9] M. Sakamoto *et al.*, *J. Nucl. Mater.* **438**, S1088 (2013).
- [10] T. Lunt *et al.*, *Phys. Rev. Lett.* **100**, 175004 (2008).